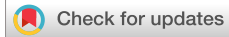


RESEARCH ARTICLE | JUNE 17 2025

Electrokinetic instabilities in Boger fluid flows with conductivity gradients

To-Lin Chen ; Md Mainul Islam ; Chase T. Gabbard; Yu-Hsiang Lee; Mahmud Kamal Raihan ; Joshua B. Bostwick ; Lung-Ming Fu ; Xiangchun Xuan  



Physics of Fluids 37, 062016 (2025)

<https://doi.org/10.1063/5.0269564>



View
Online



Export
Citation

Articles You May Be Interested In

An experimental study on the impact of Boger and Newtonian droplets on spherical surfaces

Physics of Fluids (August 2023)

Shear thickening in filled Boger fluids

J. Rheol. (March 2005)

Numerical vs experimental pressure drops for Boger fluids in sharp-corner contraction flow

Physics of Fluids (October 2016)



Physics of Fluids
Special Topics
Open for Submissions

[Learn More](#)

 AIP
Publishing

 AIP
Publishing

Electrokinetic instabilities in Boger fluid flows with conductivity gradients

Cite as: Phys. Fluids **37**, 062016 (2025); doi: [10.1063/5.0269564](https://doi.org/10.1063/5.0269564)

Submitted: 6 March 2025 · Accepted: 22 April 2025 ·

Published Online: 17 June 2025



View Online



Export Citation



CrossMark

To-Lin Chen,^{1,2} Md Mainul Islam,² Chase T. Gabbard,² Yu-Hsiang Lee,² Mahmud Kamal Raihan,² Joshua B. Bostwick,² Lung-Ming Fu,^{1,a)} and Xiangchun Xuan^{2,a)}

AFFILIATIONS

¹Department of Engineering Science, National Cheng Kung University, Tainan 70101, Taiwan

²Department of Mechanical Engineering, Clemson University, Clemson, South Carolina 29634, USA

^{a)} Authors to whom correspondence should be addressed: loudyfu@mail.ncku.edu.tw and xcxuan@clemson.edu

ABSTRACT

Electrokinetic instabilities (EKIs) occur when a sufficiently large direct current electric field interacts with a fluid flow with conductivity gradients. While EKIs in Newtonian fluids have been extensively studied for microfluidic applications such as micromixing and sample stacking, the impact of fluid rheology has not been thoroughly explored. This work reports an experimental study on how fluid elasticity affects EKI in hyaluronic acid (HA) solutions that are essentially Boger fluids under experimental conditions. It is found that increasing HA concentration (i.e., more viscoelastic) raises the threshold electric field for the onset of EKI, leading to a higher critical electric Rayleigh number. This observation indicates the suppression effect of fluid elasticity on EKI, which validates a recent numerical prediction based on the Oldroyd-B model [Sasmal, “Fluid viscoelasticity suppresses chaotic convection and mixing due to electrokinetic instability,” Phys. Fluids **34**, 082011 (2022)]. Increasing the fluid elasticity also weakens the magnitude of EKI waves but has an insignificant influence on the wave speed and frequency, in contrast to the increasing electroosmotic velocity in higher-concentration HA solutions.

© 2025 Author(s). All article content, except where otherwise noted, is licensed under a Creative Commons Attribution (CC BY) license (<https://creativecommons.org/licenses/by/4.0/>). <https://doi.org/10.1063/5.0269564>

I. INTRODUCTION

In the last thirty years, there has been a significant increase in the demand for efficient microfluidic mixing in fields such as chemical processing, biological studies, and microdevice applications.^{1–4} Many of these applications rely on an external mechanical device, such as syringe pump, to drive the fluid flow, where another external force field (e.g., acoustic, electric and magnetic fields) created by auxiliary equipment is often needed to break the otherwise diffusion-based mixing at the microscale.^{5–8} The phenomenon of electrokinetic instabilities (EKIs) has been demonstrated to mix fluids of different properties without any moving parts.^{9–11} EKIs arise from the action of electric field upon fluid conductivity (and/or permittivity) gradients,¹² which creates an electric body force drawing disturbances to the interfacial electroosmotic flow.^{13–15} These convective disturbances, if strong enough, manifest in the form of periodic or even chaotic waves, which can improve the mixing efficiency without the need for a mechanical device or auxiliary equipment.^{16–18} However, EKIs are sensitive to surface interactions (including both the wall–fluid and fluid–fluid interfaces) due to the surface-driven nature of electroosmotic flows,^{19–22} which can present challenges to the system control. Variations in

channel configurations^{23–26} and fluid properties^{27–30} have been reported to contribute to the factors that can cause inconsistency within the flow field. In addition, Joule heating has been found to play a strong role in the onset and development of EKI waves³¹ because the induced temperature gradients alter fluid properties.³²

Previous studies have mainly focused on EKI in Newtonian fluids despite the fact that many of the chemical (e.g., colloidal suspension and polymer solution) and biological (e.g., blood and urine) samples in microfluidic applications are complex fluids exhibiting non-Newtonian characteristics.^{33–39} Exploring the effects of fluid rheological properties on EKI is an emerging area of research with a significant potential for sample mixing in chemical and biomedical microdevices. Our group has reported the first study of EKI in viscoelastic polyethylene oxide (PEO) solutions.⁴⁰ As the addition of neutral PEO molecules was found to substantially reduce the electroosmotic flow,⁴¹ we had to use a syringe pump to drive the fluid through the microchannel. It was observed that increasing the PEO concentration leads to first a decrease and then an increase in the threshold electric field for the onset of EKI waves. A similar non-monotonic trend was also observed for the wave speed and frequency.⁴⁰ Such a trend was not predicted by

the numerical model of Sasmal,⁴² where the fluid elasticity effect was considered using the Oldroyd-B model.⁴³ In his simulation, Sasmal⁴² fixed the values of the electric Rayleigh and Reynolds numbers as well as the electric conductivity ratio and electric field strength. He reported a suppressed EKI when the Weissenberg number or polymer-to-solvent viscosity ratio increases. In another numerical paper, Hamid and Sasmal⁴⁴ studied EKI in power-law fluids and predicted the threshold electric field to decrease with increasing shear thinning effect. This analysis has been validated by our recent experiment of EKI in shear thinning xanthan gum (XG) solutions, where the critical electric Rayleigh number decreased with increasing XG concentration.⁴⁵ Here, shear thinning indicates that the fluid viscosity decreases with the increasing shear rate, whereas the opposite is true for shear thickening.⁴⁶ Additionally, there are a handful of studies on viscoelastic instabilities in the electroosmotic flow of polymer solutions without conductivity gradients.^{47–50} Interestingly, such electro-elastic instabilities do not necessarily enhance electroosmotic mixing.⁴⁸

In this work, we revisit experimentally the effect of fluid elasticity on EKI with the aim to compare against the numerical prediction from Sasmal.⁴² To isolate the elasticity effect from shear thinning, we use Boger fluids that are elastic fluids with constant viscosity.⁵¹ We mixed a small amount of hyaluronic acid (HA) polymer into Newtonian buffer solutions to prepare weakly viscoelastic Boger fluids, whose shear thinning behavior was found negligible under the range of shear rates typical to electroosmotic flows. HA is widely found in biological fluids with potential applications in tissue engineering, drug delivery, and biomedical microdevices.^{52,53} Moreover, as HA is a negatively charged polysaccharide and does not suppress the surface charge of microchannel walls, a syringe pumping of the fluid, which was necessary in our previous experiment of EKI in neutrally charged PEO solutions,⁴⁰ is no longer needed. We investigate how the addition of HA polymer and the increase in HA concentration change the threshold electric field for the onset of EKI waves and the wave properties. We also employ the critical electric Rayleigh number, which was proposed in our recent paper to account for the variation of fluid properties in shear thinning XG solutions,⁴⁵ to examine the overall impact of fluid elasticity on EKI and hopefully validate Sasmal's numerical prediction.⁴² The findings from this work along with those obtained in our recent paper⁴⁵ are envisioned to provide a foundation for future experimental and numerical investigations into the role of fluid rheology in the electroosmotic flow of more complex fluids.

II. EXPERIMENT

A. Materials

Figure 1(a) shows a picture of the T-shaped microchannel, which was fabricated with polydimethylsiloxane (PDMS) using the standard soft lithography technique as detailed elsewhere.²⁹ The channel has two 100 μm wide side branches and one 200 μm wide main branch joining at the T-junction with a uniform depth of 53 μm . The total length from the inlet reservoir of either side branch to the outlet reservoir of the main branch is 18 mm. All reservoirs were made large with 6-mm diameter each to minimize the potential influence of the hydrostatic pressure-driven backflow because of the electroosmotic fluid depletion and buildup in the inlet and outlet reservoirs, respectively. The microchannel was primed with de-ionized water immediately after being bonded to a glass slide. HA polymer (molecular weight, $M_w = 0.357$ MDa, Lifecore Biomedical LLC) was dissolved into 2 and

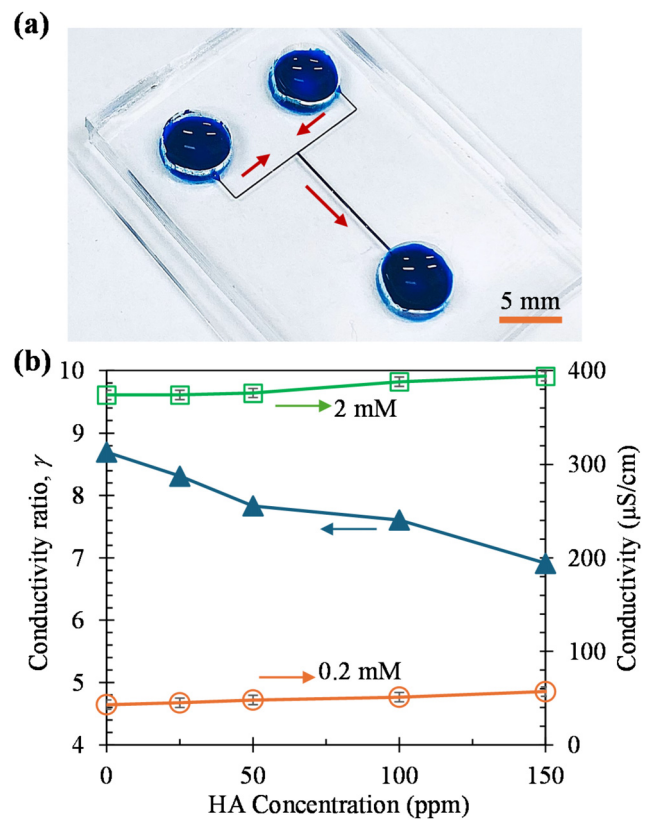


FIG. 1. (a) Picture of the T-shaped microchannel (filled with blue dye for clarity), where the arrows indicate the electroosmotic flow directions in the EKI experiment; (b) experimentally measured electric conductivities of 2 and 0.2 mM buffer-based HA solutions and the calculated conductivity ratio, γ , between them. The lines are used to guide the eyes only. The error bars for the conductivity data ($\pm 5 \mu\text{S/cm}$ at most) are within the size of markers.

0.2 mM phosphate buffer solutions in equal amounts to prepare viscoelastic fluids. The HA concentration was 25, 50, 100, and 150 ppm. The HA-free Newtonian buffer solution was also tested as the control experiment. The electric conductivities of the prepared buffer and HA solutions were measured using a conductivity meter (Fisher Scientific, Accumet AP85). As viewed from the plot in Fig. 1(b), the conductivity ratio, γ , of 2 to 0.2 mM buffer-based HA solutions decreases from 8.70 to 6.91 when the HA concentration increases from 0 (i.e., Newtonian buffers) to 150 ppm. This decreasing trend arises from the polymer addition-induced slight increase in the conductivity of both types of solutions, consistent with the observation in our previous experiments with polymer solutions.^{40,45}

The relaxation times of the prepared HA solutions were estimated from the reported value of $\lambda = 0.11$ ms for $c = 700$ ppm, $M_w = 0.9$ MDa HA solution⁵⁴ via the following molecular weight and concentration scaling:^{55,56}

$$\lambda \propto M_w^{1.8} c^{0.8}. \quad (1)$$

The elasticity effect of HA solutions is characterized by the elasticity number,⁵⁷

$$El = \frac{\lambda\mu(h+d)}{4\rho h^2d}, \quad (2)$$

where μ is the fluid viscosity, ρ is the fluid density (assumed equal to that of water because of the low polymer concentration), h is the half width of the main branch, and d is the half depth of the microchannel. The dynamic viscosities of 0.2 mM buffer-based HA solutions were measured using a cone-plate rheometer (Anton Paar, MCR 302) at room temperature. They were assumed to not deviate significantly from those of 2 mM buffer-based HA solutions according to our recent measurements of XG solutions.⁴⁵ The cone and plate of our rheometer have a diameter of 50 mm, and the cone has an angle of 1°. This geometry is the largest standard size offered for our rheometer and is designed to enhance torque sensitivity for low viscosity measurements. Shear rate sweeps were performed in the sample of each solution for shear rates ranging from 10 to 1000 1/s at $23 \pm 0.5^\circ\text{C}$. As demonstrated in Fig. 2(a), each of our prepared HA solutions can be viewed

as a Boger fluid with a constant viscosity for shear rates of no more than 120 1/s (marked by the vertical dashed line). This upper limit is seen from Fig. 2(b) to remain valid over the range of shear rates encountered in our experiments, which were estimated from the experimentally measured electroosmotic velocity, U_{eo} , of 0.2 mM buffer-based 50 ppm HA solution via the average shear rate, $2U_{eo}/h$. Table I summarizes the rheological properties and elasticity numbers of 0.2 mM buffer-based HA solutions. Increasing the polymer concentration increases both the fluid viscosity and relaxation time, leading to a stronger elasticity effect in terms of a greater El . As $El \ll 1$, all our prepared HA solutions can be viewed weakly viscoelastic in the T-shaped microchannel.

B. Methods

Prior to experiment, the priming de-ionized water was removed from the reservoirs of the T-shaped microchannel. Next, 2 and 0.2 mM buffer-based HA solutions (including HA-free solutions in the control experiment) of equal volume were dispensed into the inlet reservoirs of the two side branches, respectively. Immediately following that, the same volume of 0.2 mM buffer solution was dispensed into the outlet reservoir of the main branch for balancing the liquid height in the inlet reservoirs and hence removing the hydrostatic pressure-driven flow. Then, a platinum electrode was inserted into the solution in each of the three reservoirs. The two inlet electrodes were connected in parallel with a DC power source (Glassman High Voltage) and the outlet reservoir was grounded, which supplied an equal constant DC electric field to each side branch pumping the two solutions together through the main branch. The imposed DC voltages were kept no more than 900 V for limiting the maximum electric field to 500 V/cm on average over the 1.8 cm channel length. Moreover, every test was run for no more than one minute. These constraints helped reduce the effects of both Joule heating, which was confirmed by monitoring a no more than 10% increase in electric current during our tests,⁵⁸ and hydrostatic pressure-driven backflow as noted earlier, which was calculated to be no more than $5 \mu\text{m/s}$ in any test.

To visualize the interfacial behavior, we mixed 2 mM buffer-based solution with $50 \mu\text{M}$ Rhodamine B dye (Sigma-Aldrich). The dynamics of the fluid interface was recorded at the T-junction of the microchannel using an inverted fluorescent microscope (Nikon Eclipse TE2000U, Nikon instrument) through a FITC Hy Q filter cube (excitation at 460–500 nm, emission at 510–560 nm). Digital images were taken by a CCD camera (Nikon DS-Qi1Mc) at around 10 frames per second with an exposure time of 70 ms. The camera was switched on once the DC electric field was applied, such that both the onset and

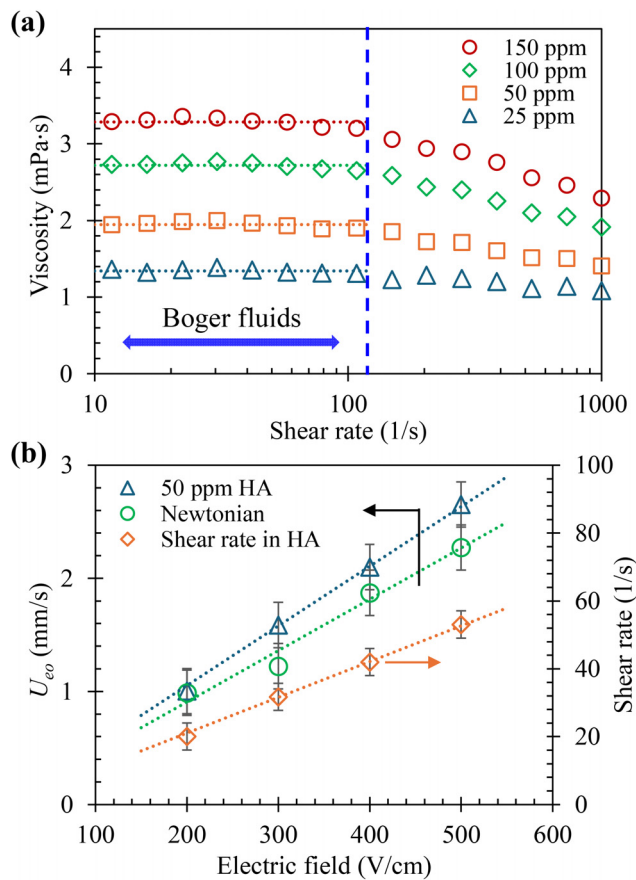


FIG. 2. (a) Experimentally measured dynamic viscosities of 0.2 mM buffer-based HA solutions, where the vertical dashed line marks the upper limit of fluid shear rate at 120 1/s for each of the HA solutions being safely viewed as a Boger fluid with a constant viscosity (see the dotted trendlines); (b) experimentally measured electroosmotic velocities, U_{eo} , of 0.2 mM buffer-based Newtonian and 50 ppm HA solutions and the calculated average shear rate in the HA solution, $2U_{eo}/h$, over a range of direct current (DC) electric fields. The dotted lines are all linear trendlines fitted to the data points with the intercept at the origin.

TABLE I. Rheological properties and elasticity numbers, El , of the prepared 0.2 mM buffer-based HA solutions. The values of dynamic viscosity η are extracted from the experimental data for shear rates no more than 120 1/s in Fig. 2(a), those of relaxation time, λ , are calculated from Eq. (1), and those of El are calculated from Eq. (2).

c (ppm)	μ (mPa s)	λ (μs)	El ($\times 10^{-3}$)
25	1.34	1.46	0.233
50	1.95	2.53	0.589
100	2.72	4.41	1.43
150	3.29	6.10	2.39

development of EKI waves were recorded. The time and location at which the first EKI wave was discerned in the view field were defined as the onset time and location of EKI waves, respectively. Images were post-processed using the Nikon imaging software (NIS-Elements AR 2.30). The amplitude of EKI waves was defined as half of the average distance measured from the valley to the summit. The speed was determined by tracking the valley of individual EKI waves with time. The frequency was obtained by counting the number of occurrences of EKI waves within a time span. The electroosmotic velocity, U_{eo} , was measured using the so-called electric current monitoring method,⁵⁹ which relies on the time response of the electric current when a test buffer solution is electroosmotically displaced by the same solution with a slightly lower (10% in our test) ionic concentration.

We employed the critical electric Rayleigh number, $Ra_{e,cr}$, to quantify the influence of fluid elasticity on EKI. This dimensionless number was introduced by Chen *et al.*¹⁴ to characterize the onset of convective EKI in Newtonian fluid flows with conductivity gradients, which measures the relative importance of dynamic electric body force to dissipative diffusion force,

$$Ra_{e,cr} = \Gamma \frac{h \varepsilon E_{th}^2 d^2}{\delta \mu D}. \quad (3)$$

In the definition, $\Gamma = (\gamma - 1)^2 / (\gamma + 1)^2$ accounts for the influence of conductivity gradients with γ being the conductivity ratio of the higher to lower conductivity fluids in Fig. 1(b), δ is the diffusion length of ions, ε is the fluid permittivity, E_{th} is the threshold electric field for the onset of EKI, and D is the effective diffusivity of ions. We revised in our recent paper⁴⁵ the definition of $Ra_{e,cr}$ by incorporating the variations of fluid properties, and proposed to use the following ratio to examine the effect of fluid shear thinning on EKI:

$$\frac{Ra_{e,cr}}{Ra_{e,cr,0}} = \left(\frac{\Gamma}{\Gamma_0} \right) \sqrt{\left(\frac{\mu}{\mu_0} \right) \left(\frac{U_{eo}}{U_{eo,0}} \right) \left(\frac{E_{th}}{E_{th,0}} \right)^2}. \quad (4)$$

In the above expression, $Ra_{e,cr,0}$ is the critical electric Rayleigh number in the Newtonian fluid (i.e., the solvent of the non-Newtonian fluid) of viscosity μ_0 , $\Gamma_0 = (\gamma_0 - 1)^2 / (\gamma_0 + 1)^2$ with γ_0 being the conductivity ratio in the Newtonian fluid (see Fig. 1), $U_{eo,0}$ and $E_{th,0}$ are the electroosmotic velocity and threshold electric field in the Newtonian fluid, respectively. It is admitted that the definition of $Ra_{e,cr}$ in Eq. (3) is only valid for Newtonian fluids. However, as Chen *et al.*¹⁴ demonstrated in their paper, the value of $Ra_{e,cr}$ remains unchanged or changes very little when the conductivity ratio or any material property (e.g., fluid density, fluid permittivity, zeta potential, ion diffusivity) is varied. Therefore, any significant change of $Ra_{e,cr}$ and in turn the ratio of $Ra_{e,cr}$ to $Ra_{e,cr,0}$ in Eq. (4) observed in our experiment with viscoelastic HA solutions can be viewed as the consequence of fluid elasticity. For convenience, we term this ratio as the Rayleigh ratio in the remainder of this paper.

III. RESULTS AND DISCUSSION

A. Comparison of EKI in Newtonian and viscoelastic fluids

Figure 3 compares the experimental images of EKI waves in Newtonian (HA-free) and viscoelastic (50 ppm HA) fluids at the T-junction of the microchannel. The threshold electric field for the onset of EKI is $E_{th} = 344$ V/cm in the viscoelastic fluid, 17% greater

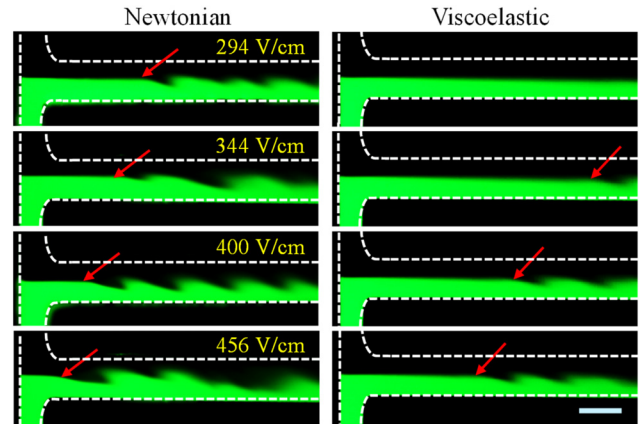


FIG. 3. Comparison of the interfacial behaviors in the electroosmotic flow of 0.2 mM (dark) and 2 mM (dye) buffer-based Newtonian (0 ppm HA, left column) and viscoelastic (50 ppm HA, right column) fluids under varying electric fields, with EKI onset observed at 344 V/cm in the viscoelastic fluid. The arrow on each image indicates the onset location of EKI waves. The dashed lines highlight the channel walls, and the scale bar represents 200 μm for both types of fluid at 344 V/cm. Multimedia available online.

than $E_{th,0} = 294$ V/cm in the Newtonian fluid. The onset location of EKI is pushed further away from the T-junction in the viscoelastic fluid. Also delayed is the onset time of EKI waves (this aspect will be revisited in Sec. III B), which take place several seconds after the application of the threshold electric field contrasting the immediate occurrence in the Newtonian fluid. These observations together indicate the fluid elasticity-induced suppression of EKI, which, as explained in Sec. III B in terms of the Rayleigh ratio in Eq. (4), is consistent with the numerical prediction of Sasmal.⁴² Such an impact is opposite to our recently reported fluid shear thinning-enhanced EKI in XG solutions.⁴⁵ Increasing the electric field strengthens the EKI waves and shifts them upstream toward the T-junction in both the Newtonian and viscoelastic fluid flows. However, the wave amplitude in the viscoelastic fluid is smaller than that in the Newtonian fluid under the same electric field. This phenomenon was also observed in our recent experiment with shear-thinning XG solutions,⁴⁵ likely due to the polymer addition-induced increase in fluid viscosity and hence viscous damping effect.

Figure 4 presents a quantitative comparison of the properties of EKI waves in the Newtonian and viscoelastic fluids, which were obtained by tracking individual waves with time on sequential images (see, for example, the arrow on each image in Fig. 3, which points to the first EKI wave propagating downstream along with the flow). As illustrated in Fig. 4(a), the wave speeds in both cases increase almost linearly with the increasing electric field. They, however, do not differ significantly from each other for the range of electric fields tested, in contrast to the observation of a noticeably faster electroosmotic flow in the HA solution in Fig. 2(b). This mismatch phenomenon was not observed in our recent study of fluid shear thinning effects on EKI.⁴⁵ Figure 4(b) compares the wave amplitudes in the two types of fluids, which, similar to the EKI waves in shear thinning fluids,⁴⁵ also exhibit an approximately linear increase with the applied electric field. However, introducing fluid elasticity reduces the wave amplitude by about 30% because of the polymer addition-enhanced viscous

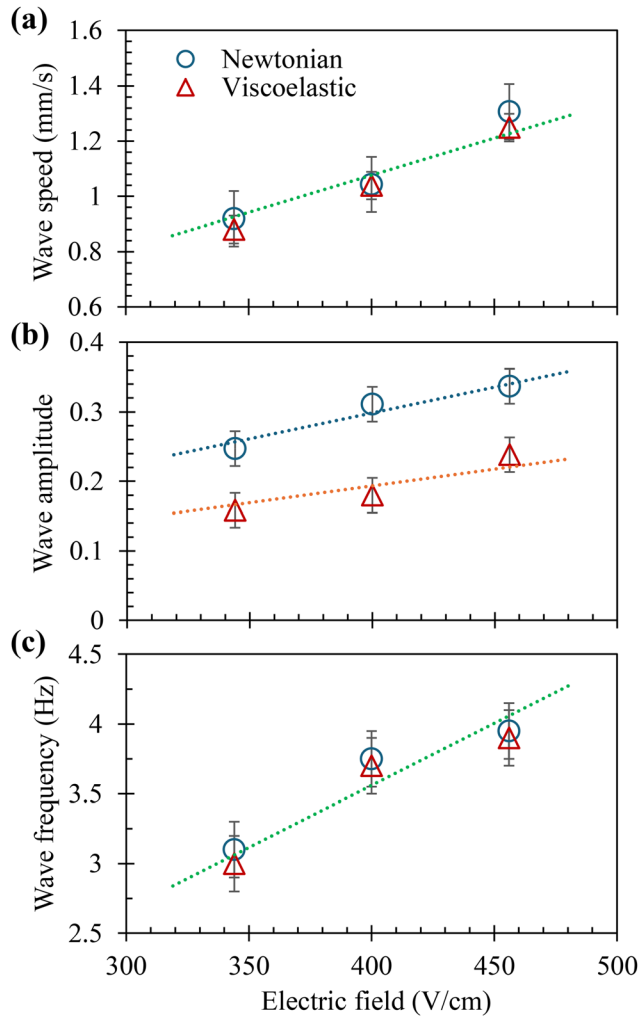


FIG. 4. Comparison of the experimentally determined properties of EKI waves in Newtonian (0 ppm HA) and viscoelastic (50 ppm HA) fluid flows: (a) wave speed; (b) wave amplitude (normalized by the half width of the main branch); and (c) wave frequency. The dotted lines are all linear trendlines fitted to the experimental data points with the intercept at the origin.

damping as noted above. Figure 4(c) compares the wave frequencies in the two fluids, which follow a roughly linear but identical profile. This trend is qualitatively similar to that for the wave speed in Fig. 4(a). Numerical studies (including theoretical such as the stability analysis of EKI¹⁴ and electroosmotic flow⁶⁰ in non-Newtonian fluids)⁶¹ are needed to understand why fluid elasticity affects only the amplitude of EKI waves, not the speed or frequency. It is unclear to the authors if the polymer-induced fluid elasticity and viscosity increase in the HA solution as compared to the Newtonian fluid are each an important factor in these observed phenomena.

B. Effect of polymer concentration

Figure 5(a) shows the experimental images of EKI waves that were each taken under the threshold electric field, E_{th} , as the HA

concentration was changed from 25 to 150 ppm. Two trends are observed from these images along with that in the Newtonian fluid (i.e., 0 ppm HA) under E_{th} in Fig. 3. One trend is the continuously increasing E_{th} from nearly 300 V/cm in 0 ppm to over 450 V/cm in 150 ppm HA solution, following a roughly linear profile as illustrated in Fig. 5(b). This trend arises from the different variations of fluid properties with the increasing HA concentration: (1) increased fluid elasticity in terms of the increasing elasticity number, El , in Table I, which is not reflected in the Rayleigh ratio in Eq. (4); (2) decreased electric conductivity ratio in Fig. 1(b), which reduces the value of Γ in Eq. (3) and in turn the Rayleigh ratio; (3) increased fluid viscosity in Fig. 2(a), which increases the Rayleigh ratio. The other trend directly observed from the images in Fig. 5(a) is that the onset location of EKI progressively shifts downstream as the HA concentration increases. Additionally, the onset time of EKI waves after the application of the threshold electric field is further delayed, which, as shown in Fig. 5(b), jumps from 0 s (i.e., no time delay) in the Newtonian fluid to nearly 7 s in 25 ppm HA solution and then increases linearly to a little over 9 s in 150 ppm HA solution.

To quantify the influence of fluid elasticity on EKI using the Rayleigh ratio in Eq. (4), we measured the electroosmotic velocity, U_{eo} , of 2 mM buffer-based Newtonian and HA solutions for electric fields ranging from 200 to 500 V/cm. We then used the experimental data of U_{eo} vs electric field to determine the electroosmotic mobility from the slope and multiply it by the threshold electric field, E_{th} , to obtain the corresponding U_{eo} in each HA solution. This treatment assumed a linear dependence of U_{eo} on electric field, which is validated by the linear trendline in Fig. 2(b) for 50 ppm HA solution. Figure 6 presents the calculated Rayleigh ratio defined in Eq. (4) for the onset of EKI in HA solutions with varying polymer concentrations. Also shown in this figure is the critical Weissenberg number, Wi_{cr} ,

$$Wi_{cr} = \frac{2\lambda U_{eo}}{h}, \quad (5)$$

which was calculated using the above obtained U_{eo} at the threshold electric field, E_{th} , in each HA solution and is another dimensionless number characterizing the fluid elasticity effect. We see from Fig. 6 that increasing the HA concentration causes an increase in the value of Wi_{cr} for the onset of EKI waves. It also continuously increases the Rayleigh ratio from 1 in the Newtonian fluid to almost 7 in 150 ppm HA solution. These trends together indicate the suppression effect of fluid elasticity on EKI, which agrees with the numerical prediction of Sasmal using the Oldroyd-B model.⁴² Such suppression effect of fluid elasticity is, however, opposite to the enhancement effect of fluid shear thinning on EKI that was observed in both our recent experiment with XG solutions⁴⁵ and Hamid and Sasmal's simulation using the power-law model.⁴⁴

Figure 7(a) compares the experimental images of EKI waves in HA solutions ranging from 25 to 150 ppm under a constant electric field of 456 V/cm. This electric field, which is the E_{th} for the onset of EKI in 150 ppm HA solution, was chosen to ensure that EKI can take place in all the HA solutions. As the HA concentration increases, the EKI waves initiate at a location further away from the T-junction with an apparently smaller amplitude. As seen from Fig. 7(b), the wave amplitude (relative to the half width of the main branch) reduces from 0.31 in the Newtonian fluid to 0.20 in 150 ppm HA solution by about 35% because of the increasing influences of both viscous damping and

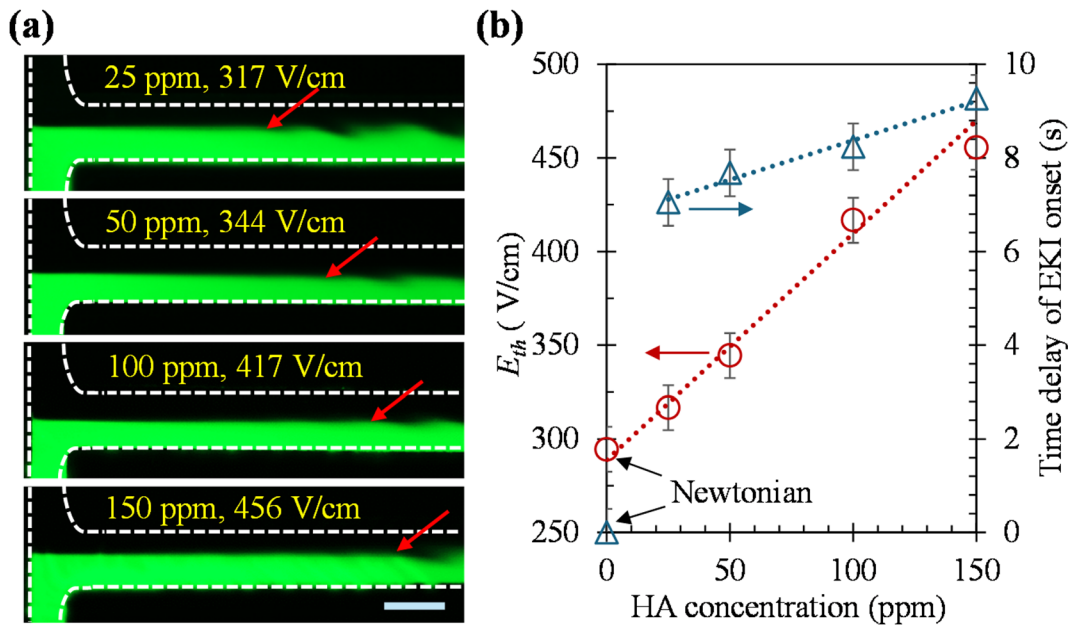


FIG. 5. EKI in 0.2 mM (dark) and 2 mM (dyed) buffer-based viscoelastic fluids with varying HA concentrations: (a) experimental images of the interfacial behavior under respective threshold electric fields, E_{th} , where the arrows indicate the onset location of EKI waves; (b) plot of E_{th} and the delay for the onset time of EKI waves vs HA concentration. The dashed lines in (a) highlight the channel walls and the scale bar represents 200 μm.

elastic suppression. In contrast, the measured wave speed and frequency in Fig. 7(c) remain almost unchanged at $1.26 (\pm 0.04)$ m/s and $3.92 (\pm 0.08)$ Hz, respectively, over the range of HA concentrations. Each of these trends appears to agree with the observation in Fig. 4 for the EKI wave speed and frequency in between the Newtonian buffer and 50 ppm HA solutions under varying electric fields. They all, however, differ from the non-monotonic dependences of wave properties on polymer concentration for EKI in shear thinning XG solutions.⁴⁵ Figure 7(c) also shows the measured electroosmotic velocity, U_{eo} , in

HA solutions, which increases at higher HA concentrations under a constant electric field despite the increase in fluid viscosity [see Fig. 2(a)]. This trend is opposite to our recently reported decreasing U_{eo} in higher-concentration shear thinning XG solutions.⁴⁵ It also contrasts with the almost constant wave speed in viscoelastic fluids in Fig. 7(c) regardless of the HA concentration. Table II summarizes the comparison of the fluid rheological properties and effects on EKI in this work with viscoelastic HA solutions and our recent paper with shear thinning XG solutions,⁴⁵ where the Newtonian buffer is used as the reference.

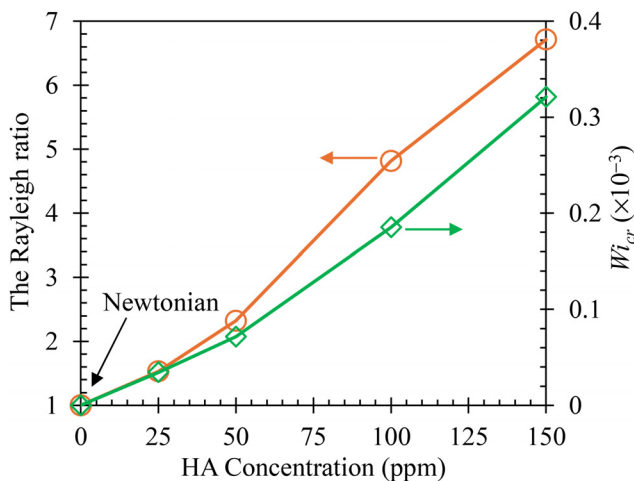


FIG. 6. Plot for the calculated Rayleigh ratio in Eq. (4), whose increasing trend with the HA concentration is consistent with that of the calculated critical Weissenberg number, Wi_{cr} , in Eq. (5). The lines are used to guide the eyes only.

IV. CONCLUSIONS

We have experimentally studied the onset and development of EKI waves in weakly viscoelastic HA solutions that can be safely viewed as Boger fluids under our experimental conditions. We find that increasing the HA concentration from 0 to 150 ppm continuously raises the threshold electric field for the onset of EKI from 317 to 456 V/cm by more than 40%. Accordingly, the ratio of the calculated critical electric Rayleigh number in the HA solution to that in the Newtonian fluid increases from unity to nearly seven. These phenomena indicate the fluid elasticity-induced strong suppression effect on EKI, which validates the numerical prediction from Sasmal on EKI in Oldroyd-B fluids.⁴² We have also conducted a detailed analysis of the properties of EKI waves in both the Newtonian and viscoelastic fluids under a fixed electric field. Increasing the HA concentration reduces the wave magnitude while the wave speed and frequency show minimal variations, different from the increasing electroosmotic velocity. Our research highlights the critical role of fluid elasticity in modulating electrokinetic behavior and provides valuable experimental data for understanding the rheological effects on EKI in non-Newtonian fluids. In future work, we will expand experiments to test different fluid

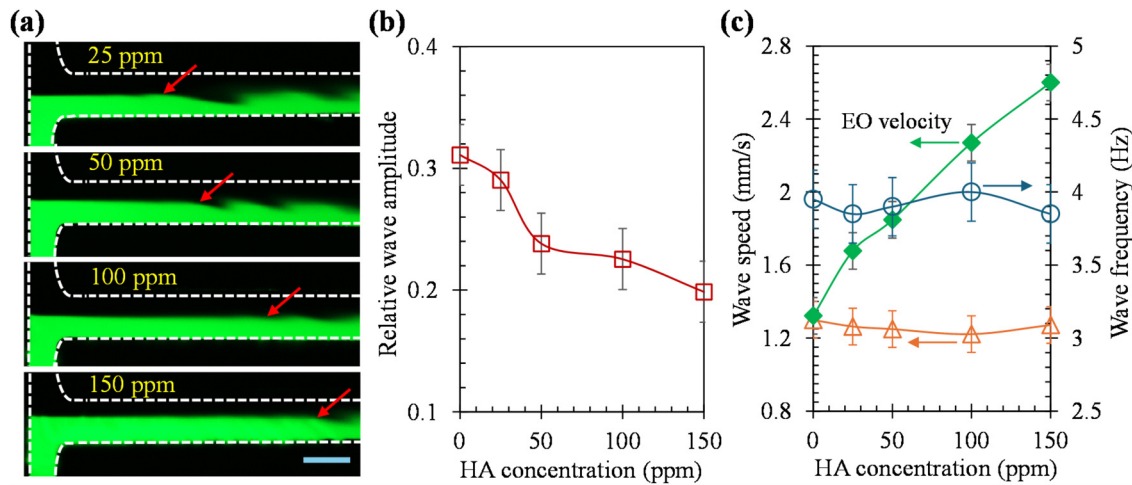


FIG. 7. Effect of HA concentration on EKI waves under the electric field of 456 V/cm: (a) experimental images on which the arrows each indicate where the EKI waves first start, the dashed lines highlight the channel walls, and the scale bar represents 200 μm; (b) wave amplitude (related to the half width of the main branch); (c) wave speed and frequency along with the experimentally measured electroosmotic (EO) velocity of 2 mM buffer-based HA solutions. The lines in (b) and (c) are used to guide the eyes only. The dashed lines in (a) highlight the channel walls and the scale bar represents 200 μm.

TABLE II. Comparison of the fluid rheological properties and effects on EKI in viscoelastic HA and shear thinning XG solutions. All trends listed for both polymer solutions are based upon the Newtonian buffer when the polymer concentration increases.

Property	HA solutions (this study)	XG solutions (Ref. 45)
Rheology	Elasticity	Shear thinning
Dimensionless number for rheological properties	El increases	Power-law index decreases
E_{th}	Increase	Decrease
Dealy of onset time	Increase	No
Shift of onset location	Further downstream	Further upstream
$Ra_{e,cr}$	Increase	Decrease
Dimensionless number for rheological effects	Wi_{cr} increases	Re_{cr} decreases
U_{eo}	Increase	Decrease
Wave speed	Nearly constant	Non-monotonic
Wave amplitude	Decrease	Non-monotonic
Wave frequency	Nearly constant	Non-monotonic

configurations, including one Newtonian and one non-Newtonian fluid, for a deeper understanding of electro-elastic instabilities.⁶² We also hope to see more numerical studies on the effects of fluid rheological properties⁶¹ in EKI to explain the experimental results in both this work and our recent work with shear thinning fluids.⁴⁵

ACKNOWLEDGMENTS

This work was supported in part by NSF under Grant Nos. CBET-2100772 and CBET-2127825 (X.X.), and by Clemson University through the Creative Inquiry Program (X.X.).

AUTHOR DECLARATIONS

Conflict of Interest

The authors have no conflicts to disclose.

Author Contributions

To-Lin Chen: Data curation (lead); Formal analysis (equal); Investigation (lead); Methodology (equal); Visualization (lead); Writing – original draft (lead). **Md Mainul Islam:** Data curation (supporting); Investigation (supporting); Visualization (supporting); Writing – review & editing (supporting). **Chase T. Gabbard:** Data curation (supporting); Investigation (supporting); Writing – review & editing (supporting). **Yu-Hsiang Lee:** Investigation (supporting); Visualization (supporting). **Mahmud Kamal Raihan:** Data curation (supporting); Formal analysis (equal); Methodology (equal); Writing – review & editing (supporting). **Joshua B. Bostwick:** Conceptualization (equal); Funding acquisition (equal); Project administration (supporting); Resources (equal); Supervision (supporting); Writing – review & editing (supporting). **Lung-Ming Fu:** Conceptualization (equal); Funding acquisition (equal); Project administration (supporting);

Resources (equal); Supervision (supporting); Writing – original draft (supporting); Writing – review & editing (supporting). **Xiangchun Xuan**: Conceptualization (equal); Funding acquisition (equal); Project administration (lead); Resources (equal); Supervision (equal); Writing – review & editing (lead).

DATA AVAILABILITY

The data that support the findings of this study are available from the corresponding authors upon reasonable request.

REFERENCES

- ¹C.-Y. Lee, C.-L. Chang, Y.-N. Wang, and L.-M. Fu, “Microfluidic mixing: A review,” *Int. J. Mol. Sci.* **12**, 3263–3287 (2011).
- ²M. B. Khan, F. Hamid, N. Ali, V. Mehandia, and C. Sasmal, “Flow-switching and mixing phenomena in electroosmotic flows of viscoelastic fluids,” *Phys. Fluids* **35**, 083101 (2023).
- ³Y. Wei, Y. Chen, J. Xu, and J. Li, “Induced charge electro-osmotic mixing performance of viscoelastic fluids in microchannels with an electrically conductive plate,” *Phys. Fluids* **35**, 083102 (2023).
- ⁴M. Khatibi, S. K. Mehta, S. N. Ashrafzadeh, and P. K. Mondal, “Surface charge-dependent slip length modulates electroosmotic mixing in a wavy micromixer,” *Phys. Fluids* **36**, 073105 (2024).
- ⁵C.-Y. Lee, W.-T. Wang, C.-C. Liu, and L.-M. Fu, “Passive mixers in microfluidic systems: A review,” *Chem. Eng. J.* **288**, 146–160 (2016).
- ⁶S. Cai, Y. Jin, Y. Lin, Y. He, P. Zhang, Z. Ge, and W. Yang, “Micromixing within microfluidic devices: Fundamentals, design, and fabrication,” *Biomicrofluidics* **17**, 061503 (2023).
- ⁷C.-Y. Lee and L.-M. Fu, “Recent advances and applications of micromixers,” *Sens. Actuators, B* **259**, 677–702 (2018).
- ⁸S. M. Saravanakumar and P.-V. Cicek, “Microfluidic mixing: A physics-oriented review,” *Micromachines* **14**, 1827 (2023).
- ⁹M.-Z. Huang, R.-J. Yang, C.-H. Tai, C.-H. Tsai, and L.-M. Fu, “Application of electrokinetic instability flow for enhanced micromixing in cross-shaped microchannel,” *Biomed. Microdev.* **8**, 309–315 (2006).
- ¹⁰H. Lin, “Electrokinetic instability in microchannel flows: A review,” *Mech. Res. Commun.* **36**, 33–38 (2009).
- ¹¹J. Park, S. M. Shin, K. Y. Huh, and I. S. Kang, “Application of electrokinetic instability for enhanced mixing in various micro-T-channel geometries,” *Phys. Fluids* **17**, 118101 (2005).
- ¹²J. R. Melcher and G. I. Taylor, “Electrohydrodynamics: A review of the role of interfacial shear stresses,” *Annu. Rev. Fluid Mech.* **1**, 111–146 (1969).
- ¹³H. Lin, B. D. Storey, M. H. Oddy, C. Chen, and J. G. Santiago, “Instability of electrokinetic microchannel flows with conductivity gradients,” *Phys. Fluids* **16**, 1922–1935 (2004).
- ¹⁴C. Chen, H. Lin, S. K. Lele, and J. G. Santiago, “Convective and absolute electrokinetic instability with conductivity gradients,” *J. Fluid Mech.* **524**, 263–303 (2005).
- ¹⁵M. H. Oddy and J. G. Santiago, “Multiple-species model for electrokinetic instability,” *Phys. Fluids* **17**, 064108 (2005).
- ¹⁶H. Lin, B. D. Storey, and J. G. Santiago, “A depth-averaged electrokinetic flow model for shallow microchannels,” *J. Fluid Mech.* **608**, 43–70 (2008).
- ¹⁷C. H. Tai, R. J. Yang, M. Z. Huang, C. W. Liu, C. H. Tsai, and L. M. Fu, “Micromixer utilizing electrokinetic instability-induced shedding effect,” *Electrophoresis* **27**, 4982–4990 (2006).
- ¹⁸J. D. Posner, C. L. Pérez, and J. G. Santiago, “Electric fields yield chaos in microflows,” *Proc. Natl. Acad. Sci. U. S. A.* **109**, 14353–14356 (2012).
- ¹⁹G. M. Whitesides and A. D. Stroock, “Flexible methods for microfluidics,” *Phys. Today* **54**(6), 42–48 (2001).
- ²⁰S. Ghosal, “Electrokinetic flow and dispersion in capillary electrophoresis,” *Annu. Rev. Fluid Mech.* **38**, 309–338 (2006).
- ²¹C. Zhao and C. Yang, “Advances in electrokinetics and their applications in micro/nano fluidics,” *Microfluid. Nanofluid.* **13**, 179–203 (2012).
- ²²D. Kumar, S. K. Mehta, and P. K. Mondal, “Enhanced bio-fluids mixing by the soft polyelectrolyte layer-modulated electroosmotic vortices,” *Phys. Fluids* **35**, 072019 (2023).
- ²³J. D. Posner and J. G. Santiago, “Convective instability of electrokinetic flows in a cross-shaped microchannel,” *J. Fluid. Mech.* **555**, 1–42 (2006).
- ²⁴K. Dubey, A. Gupta, and S. S. Bahga, “Coherent structures in electrokinetic instability with orthogonal conductivity gradient and electric field,” *Phys. Fluids* **29**, 092007 (2017).
- ²⁵B. D. Storey, B. S. Tilley, H. Lin, and J. G. Santiago, “Electrokinetic instabilities in thin microchannels,” *Phys. Fluids* **17**, 018103 (2005).
- ²⁶L. Song, L. Yu, Y. Zhou, A. R. Antao, R. A. Prabhakaran, and X. Xuan, “Electrokinetic instability in microchannel ferrofluid/water co-flows,” *Sci. Rep.* **7**, 46510 (2017).
- ²⁷G. Navaneetham and J. D. Posner, “Electrokinetic instabilities of non-dilute colloidal suspensions,” *J. Fluid Mech.* **619**, 331–365 (2009).
- ²⁸W. J. Luo, “Effect of ionic concentration on electrokinetic instability in a cross-shaped microchannel,” *Microfluid. Nanofluid.* **6**, 189–202 (2009).
- ²⁹D. T. Kumar, Y. Zhou, V. Brown, X. Lu, A. Kale, L. Yu, and X. Xuan, “Electric field-driven instabilities in ferrofluid microflows,” *Microfluid. Nanofluid.* **19**, 43 (2015).
- ³⁰L. Song, P. Jagdale, L. Yu, Z. Liu, C. Zhang, R. Gao, and X. Xuan, “Electrokinetic instabilities in co-flowing ferrofluid and buffer solutions with matched electric conductivities,” *Microfluid. Nanofluid.* **22**, 134 (2018).
- ³¹L. Song, L. Yu, C. Brumme, R. Shaw, C. Zhang, and X. Xuan, “Joule heating effects on electrokinetic flows with conductivity gradients,” *Electrophoresis* **42**, 967–974 (2021).
- ³²X. Xuan, “Review of nonlinear electrokinetic flows in insulator-based dielectrophoresis: From induced charge to Joule heating effects,” *Electrophoresis* **43**, 167–189 (2022).
- ³³G. D’Avino, G. Greco, and P. L. Maffettone, “Particle migration due to viscoelasticity of the suspending liquid and its relevance in microfluidic devices,” *Annu. Rev. Fluid Mech.* **49**, 341–360 (2017).
- ³⁴X. Lu, C. Liu, G. Hu, and X. Xuan, “Particle manipulations in non-Newtonian microfluidics: A review,” *J. Colloid Interface Sci.* **500**, 182–201 (2017).
- ³⁵C. A. Browne, A. Shih, and S. S. Datta, “Pore-scale flow characterization of polymer solutions in microfluidic porous media,” *Small* **16**, 1903944 (2020).
- ³⁶D. Chen, X. Luo, Z. Su, K. Luo, and H. Yi, “Thermal gradient and elastic dependence of induced charge electro-osmosis in viscoelastic fluids,” *Phys. Fluids* **35**, 012008 (2023).
- ³⁷S. K. Mehta, A. Ghosh, P. K. Mondal, and S. Wongwises, “Electroosmosis of viscoelastic fluids in pH-sensitive hydrophobic microchannels: Effect of surface charge-dependent slip length,” *Phys. Fluids* **36**, 023101 (2024).
- ³⁸M. K. Raihan, N. Kim, Y. Song, and X. Xuan, “Elasto-inertial instabilities in the merging flow of viscoelastic fluids,” *Soft Matter* **20**, 6059–6067 (2024).
- ³⁹J. Xu, W. Yu, C. Li, L. Hou, F. Bao, and J. Li, “Chaos-induced charge electro-osmosis of Phan-Thien-Tanner fluids around a metal cylinder,” *Phys. Fluids* **37**, 033108 (2025).
- ⁴⁰L. Song, P. P. Jagdale, L. Yu, Z. Liu, D. Li, C. Zhang, and X. Xuan, “Electrokinetic instability in microchannel viscoelastic fluid flows with conductivity gradients,” *Phys. Fluids* **31**, 082001 (2019).
- ⁴¹I. Wong and C.-M. Ho, “Surface molecular property modifications for poly(dimethylsiloxane) (PDMS) based microfluidic devices,” *Microfluid. Nanofluid.* **7**, 291–306 (2009).
- ⁴²C. Sasmal, “Fluid viscoelasticity suppresses chaotic convection and mixing due to electrokinetic instability,” *Phys. Fluids* **34**, 082011 (2022).
- ⁴³R. B. Bird, “Constitutive equations for polymer liquids,” *Annu. Rev. Fluid Mech.* **27**, 169–193 (1995).
- ⁴⁴F. Hamid and C. Sasmal, “Strong effect of fluid rheology on electrokinetic instability and subsequent mixing phenomena in a microfluidic T-junction,” *Phys. Fluids* **35**, 013107 (2023).
- ⁴⁵T. Chen, M. K. Raihan, S. M. Tabarhoseini, C. Gabbard, M. M. Islam, Y. Lee, J. Bostwick, L. Fu, and X. Xuan, “Electrokinetic flow instabilities in shear thinning fluids with conductivity gradients,” *Soft Matter* **21**, 699–707 (2025).
- ⁴⁶R. B. Bird, R. C. Armstrong, and O. Hassager, *Dynamics of Polymeric Liquids* (Wiley-Interscience, Hoboken, NJ, 1987), Vol. 1.
- ⁴⁷R. M. Bryce and M. R. Freeman, “Extensional instability in electro-osmotic microflows of polymer solutions,” *Phys. Rev. E* **81**, 036328 (2010).

- ⁴⁸R. M. Bryce and M. R. Freeman, "Abatement of mixing in shear-free elongationally unstable viscoelastic microflows," *Lab Chip* **10**, 1436–1441 (2010).
- ⁴⁹F. Pimenta and M. A. Alves, "Electro-elastic instabilities in cross-shaped microchannels," *J. Non-Newtonian Fluid Mech.* **259**, 61–77 (2018).
- ⁵⁰L. Song, L. Yu, D. Li, P. P. Jagdale, and X. Xuan, "Elastic instabilities in the electroosmotic flow of non-Newtonian fluids through T-shaped microchannels," *Electrophoresis* **41**, 588–597 (2020).
- ⁵¹D. F. James, "Boger fluids," *Annu. Rev. Fluid Mech.* **41**, 129–142 (2009).
- ⁵²S. J. Haward, A. Jaishankar, M. S. N. Oliveira, M. A. Alves, and G. H. McKinley, "Extensional flow of hyaluronic acid solutions in an optimized microfluidic cross-slot device," *Biomicrofluidics* **7**, 044108 (2013).
- ⁵³R. Hidema, T. Oka, Y. Komoda, and H. Suzuki, "Effects of flexibility and entanglement of sodium hyaluronate in solutions on the entry flow in micro abrupt contraction-expansion channels," *Phys. Fluids* **31**, 072005 (2019).
- ⁵⁴S. J. Haward, "Characterization of hyaluronic acid and synovial fluid in stagnation point elongational flow," *Biopolymers* **101**, 287–305 (2014).
- ⁵⁵M. K. Raihan, P. P. Jagdale, S. Wu, X. Shao, J. B. Bostwick, X. Pan, and X. Xuan, "Flow of non-Newtonian fluids in a single-cavity microchannel," *Micromachines* **12**, 836 (2021).
- ⁵⁶S. Wu, M. K. Raihan, L. Song, X. Shao, J. B. Bostwick, L. Yu, X. Pan, and X. Xuan, "Polymer effects on viscoelastic fluid flows in a planar constriction microchannel," *J. Non-Newtonian Fluid Mech.* **290**, 104508 (2021).
- ⁵⁷L. E. Rodd, T. P. Scott, D. V. Boger, J. J. Cooper-White, and G. H. McKinley, "The inertio-elastic planar entry flow of low-viscosity elastic fluids in micro-fabricated geometries," *J. Non-Newtonian Fluid Mech.* **129**, 1–22 (2005).
- ⁵⁸X. Xuan, "Joule heating in electrokinetic flow," *Electrophoresis* **29**, 33–43 (2008).
- ⁵⁹X. Huang, M. J. Gordon, and R. N. Zare, "Current-monitoring method for measuring the electroosmotic flow rate in capillary zone electrophoresis," *Anal. Chem.* **60**, 1837–1838 (1988).
- ⁶⁰G. C. Shit, A. Sengupta, and P. K. Mondal, "Stability analysis of electro-osmotic flow in a rotating microchannel," *J. Fluid Mech.* **983**, A13 (2024).
- ⁶¹M. A. Alves, P. J. Oliveira, and F. T. Pinho, "Numerical methods for viscoelastic fluid flows," *Annu. Rev. Fluid Mech.* **53**, 509–541 (2021).
- ⁶²A. M. Afonso, F. T. Pinho, and M. A. Alves, "Electro-osmosis of viscoelastic fluids and prediction of electro-elastic flow instabilities in a cross slot using a finite-volume method," *J. Non-Newtonian Fluid Mech.* **179–180**, 55–68 (2012).